THE INTERNATIONAL JOURNAL OF SCIENCE & TECHNOLEDGE

Application of Potential Field Data for Mapping and Delineating Geological Structural Trends of the Rufiji Depression and Its Vicinity for Hydrocarbon Exploration, Tanzania

Lucas M. Luhaga
Geophysicist, Department of Upstream Operations, Tanzania Petroleum Development Corporation (TPDC), Dar es Salaam, Tanzania
Dr. Randell A. Stephenson
Professor, Department of Geology and Petroleum Geology, School of Geosciences, University of Aberdeen, Scotland, UK

Abstract:
Rufiji Depression covers mainly the Rufiji River in the southeast of Tanzania. It is one of the coast basins of Tanzania formed during the rifting events of both the failed Karoo I in the west and successful Karoo II in the east with sediments deposition from Permian to Jurassic period. This study intended at mapping and delineating geological structural trends in this region, where potential field data were utilized. The first vertical derivative (1VDR), tilt derivative (TDR) and total horizontal derivative (THD) enhancement methods were applied to the reduction to pole of the total magnetic intensity (RTP-TMI), while the 1VDR and TDR methods were applied to gravity data. After the enhancement methods to the potential field data, the geological structural trends related to regional faults with major trends: W – E, NNW – SSE, NNE – SWW, NNW – SSE and NNE –SSW were identified and delineated. Also, some new structural trends in the Massasi Spur Basement and probably Neogene structures from gravity data were detected. The regional depth to basement was computed using Power spectrum and Standard Euler Deconvolution method for magnetic and gravity data respectively. With these methods, the depth to basement was estimated in the range of (2.3 ± 0.8 – 10.5 ± 0.8) km, across the study area. Comparison of the results with other geological studies conducted across the coast basins of Tanzania indicated good correlation. Generally, the confirmed existence of structural trends in the Rufiji Depression and its vicinity controls the deposition of sediments and acts as hydrocarbon migration pathways in this region.

Keywords*: Potential field, Rufiji depression, enhancement mechanism, structural trends, basement depth, power spectrum, Euler Deconvolution, Structural index, West Songo songo*

1. Introduction

The Rufiji Depression covers an area of ~ 21,000km^2 part of the coastal basins located in Lindi Region north, the offshore Mafia Deep Sub-Basin on the east, Mandawa Salt Basin and metamorphic basement on its south, Selous Basin on the southwest and metamorphic basement at the northwest (Hudson & Nicholas 2014). Hydrocarbon exploration has been conducted on the east part of this area with gas discoveries of resources about (2.57 TCF) trillion cubic feet in both Songo songo main Block (SSMB) and Kiliwani north-1 well while sparse and limited coverage of 2D seismic data in the West Songo songo Block (WSSB) are available.

The present study is intended to offer a better understanding of existing geological structures and sediment distribution in the Rufiji Depression by processing, analysing and interpreting regional magnetic and gravity data. Its objectives include mapping/delineating of geological structures and determining sediment thickness of the study area.

2. Tectonic Setting and Geology of the Study Area

The tectonics of the study area is brought out by the Intracontinental rifting in East Africa which originated in the northern Kenya with volcanism and fault propagation of the western and southern branches moving southward through Uganda, Tanzania to Mozambique, while the northwards propagation connected the East Africa Rift System (EARS) with the Gulf of Aden and Red Sea spreading centres, creating the Afar Triple Junction in Ethiopia at ~11 Ma (Lamotte et al. 2015 & Watson et al. 2012) as shown in Figure 2 These faults are marked by two significant trends: NNE – SSW (Tanga fault)

associated with the Karoo rifting and NNW- SSE (Lindi fault) caused by the Early Jurassic rifting (Kapilima 2002). The Mid Tertiary EARS is the latest example of tectonic impact in this region.

In reference to Figure 1 and Figure 3, the geology of the study area is characterized by the existence of kaolinitic rocks (clayey-silt kaolinitic sandstones) of the Mid-Miocene age in the Pugu Hill (Schwaighofer & Muller 1987); salt dome of the Early-Jurassic age in the Mandawa Salt Basin (Kent et al.1971; Hudson & Nicholas 2014; Said et al.2015). The area also contains some local intrusive hot spring across the Rufiji valley; dykes, sills of phonolites, dolerites and carbonatitic plugs of the Eocene age formed during the EARS towards the Matumbi Hill (Kreuser et al. 1990). Moreover, the area is covered by metamorphic and igneous rocks that extends from the Massasi Spur Basement (Kent et al. 1971; Hudson & Nicholas 2014; Said et al. 2015); intrusive igneous rocks of the Davie ridge in the Indian ocean formed during the Karoo II rift system (Causebrook and Archer 1979; Watson & et al. 2012); volcanic intrusion and carbonatite rocks cutting the Karoo of the Cretaceous age to the Northern part of the study area (Kent et al. 1971; Spence 1957).

3. Data Processing and Analysis

3.1. Magnetic Data

The digital regional airborne magnetic dataset used in this project was made available by TPDC, the data were acquired by the Geosurvey International in Tanzania regions from 1976 – 1980. The data were acquired at line spacing of 1km along the E – W flight lines, and N – S tie lines flown every 10 km at an average altitude of 120m above the terrain. The survey aimed to promote Mineral and Hydrocarbon exploration in Tanzania. The survey lines were flown E – W perpendicular to the regional structures trending N – S; N – NE and NE – SW from the known geology of Tanzania since Parmian to Miocene during the EARS (Causebrook & Archer 1979; Lamotte et al. 2015). All preliminary corrections of magnetic data were conducted by Geosurvey International where the geomagnetic gradient was eliminated using the 1980 International Geomagnetic Reference Field (IGRF) model. The data were projected to the Transverse Mecator coordinate system (WGS 84 / UTM 37S) for correlation of geological information of the study area. In the present study the aeromagnetic data were gridded at a grid cell size 200x200m equivalent to one fifth (1/5) of the survey line spacing (1000m) using minimum curvature algorithm which is the most suitable for interpolation and smoothing grid surfaces of potential field data (Briggs 1974). Hence the total magnetic intensity (TMI) map was generated Figure 4. The TMI anomaly data were then transformed to the reduced to pole (RTP) filter using Geomagnetic inclination (41°), declination (-33°) and amplitude corrections (-20). The amplitude correction value is negative because the Rufiji Depression is located to the south hemisphere of the world map. According to Reeves (2005); Sheriff (2002) and Blakely (1995) the reduction to pole is important to the TMI in order to correct for phase shifts of magnetic anomalies from the centre of their magnetic sources. A low-pass Butterworth filter (cut-off wavelength 500m, filter order 8) and an upward continued filter with distance for upward to continue 1700m both were implemented during the RTP of the TMI data. The low-pass Butterworth filter parameters were chosen after a critical evaluation of several cut-off wave-lengths and filter-orders. The Butterworth filter was applied to the TMI anomaly to attenuate short-wavelength components in the data while the upward continuation was intended to attenuate the effects of near surface sources related to deeper magnetic sources. Finally, the RTP-TMI anomaly map was produced Figure 5.

3.1.1. The first Vertical Derivative (1VDR)

The magnetic data anomalies always consist of short-wavelength (high-frequency) anomalies which are basically due to magnetic sources on the surface or shallow subsurface. In such a scenario, 1VDR filter is employed to enhance the short-wavelength (high-frequency) anomalies while attenuating the long-wavelength (low-frequency) anomalies in the magnetic data (Cooper & Cowan 2004; Telford et al. 1998). In this study the 1VDR filter was applied to the RTP-TMI in order to improve the geological resolution of short-wavelength (shallow magnetic causatives), to highlight the edges of shallow magnetic anomalies and delineate geological body contacts or boundaries (Cooper & Cowan 2004; Reeves 2005; Telford et al. 1998) within the subsurface as shown on the 1VDR map Figure 6.

Mathematically, the 1VDR expression is given as

$$1VDR = -\frac{\partial M}{\partial Z}, \qquad 1$$

Where M is the magnetic intensity (nT) and Z the ground depth in (m) while the negative sign indicates the measured depth below the ground level? The 1VDR of the RTP-TMI anomaly created was adequate to constrain the edges and boundaries of geological bodies in the study area, thus it was unnecessary to present the second vertical derivative map of the RTP-TMI anomaly in this work because the 1VDR preserved much of the improved short-wavelength than the second vertical derivative of the RTP-TMI anomaly.

3.1.2. Total Horizontal Derivatives

According to Phillips (1998), the total horizontal derivative is sometimes known as the horizontal gradient method which involves the magnitude of the horizontal derivative along the x and y axes defined as

$$THD = \sqrt{\left(\frac{\partial M}{\partial x}\right)^2 + \left(\frac{\partial M}{\partial y}\right)^2} \qquad 2$$

for gridded data, where M is the RTP-TMI data. The THD method is essentially used to produce apparent geological body contacts that are linear and very continuous in the subsurface (Phillips 2000). In this study, the RTP-TMI grid was subjected to the THD filter and the THD magnetic anomaly map was generated Figure 7.

3.1.3. The Tilt Derivative

According to Verdzco et al. (2004), tilt derivative is an arctan of the ration between the first vertical derivative (1VDR) and the total horizontal derivative (THD) defined as

$$TDR = \arctan\left(\frac{1VDR}{THD}\right) \qquad 3$$

The TDR usually applied as an alternative to the vertical derivative basically for mapping continuity or discontinuity of geological structural trends by highlighting the geomagnetic fabric. It is the most robust way of discriminating magnetic signal from noises and it is an excellent edge detection filter (Fairhead et al. 2004; Miller & Singh 1994). In the present study the TDR was applied to the RTP-TMI grid, the TDR anomaly map was created Figure 8 from which the continuity and edges of geological features are greatly accentuated as compared to the RTP-TMI anomaly Figure 5.

3.2. Gravity Data

Gravity data used in this study were provided by TPDC from Tanzania which were acquired by Agip from 1976 - 1980. The data consists of a limited digital Bouguer anomaly profiles which were acquired randomly along major transportation routes with adequate spacing for regional gravity survey. The necessary gravity data corrections were carried out by the Geological Survey of Tanzania, the Bouguer anomaly density correction was 2.1g/cc at an accuracy of 1.5mGal which is within the accuracy of gravity data estimation (3mGal) according to Stephenson & Ricketts (1990). In this work, the Bouguer anomaly data was gridded at a grid cell size 1800m using minimum curvature as an interpolation method for sparse and randomly collected data (Briggs 1974), then the Bouguer anomaly map was produced Figure 9.

3.2.1. Regional-Residual Anomaly Separation

Regional-residual anomaly isolation has been implemented by various authors using polynomial fitting method (e.g Jacoby & Smilde 2009), FFT – upward continuation method (Blakely 1995) etc. The upward continuation method provides a robust strategy of frequency separation in potential field data (Jacobson 1987). It enhances the dominance of large deeper gravity causative anomalies and produces a more visible and geologically interpretable grid than a fixed frequency or band-pass filtered grid.

In the present study, the upward continuation method was applied to the Bouguer anomaly data after been fitted with a second order polynomial filter (Atawa 2016) at distance for upward continuing filter 6000m to generate the regional gravity anomaly Figure 10 which was subsequently subtracted from the original Bouguer anomaly (BA) to produce the residual gravity anomaly Figure 11. The distance for an upward continuation filter (6000m) was chosen as it enhanced the dominance of large deeper gravity causative anomalies than other several tested parameters in this study.

3.2.2. Gravity Anomaly Enhancement

The first vertical derivative (Cooper & Cowan 2004; Reeves 2005; Telford et al. 1998) and tilt derivative (Verdzco et al., 2004) methods were applied to the residual anomaly grid to detect edges contacts of geological features like faults, tilted blocks, doming features existing in the study area Figure 12 and Figure 13.

3.3. Determination of Basement Depth

3.3.1. Power Spectrum Method

Power spectrum method is one of the most efficient methods used to compute depth to magnetic sources (Spector and Grant, 1970; Connard et al., 1983). The depth to magnetic sources equation by Nayak & Petkovic (2011); Geosoft Inc (2015) is given as;

$$h = \frac{1}{4\pi}\left(\frac{\Delta E}{\Delta N}\right), \qquad 4$$

Where E = energy in log power,

N = Frequency/wave-number and $\frac{\Delta E}{\Delta N}$ is the slope of the radially averaged power spectrum. This method uses minimum widow size to constrain the source depth to basement in the survey area. The selection of optimum window size for this method has been reviewed by several authors (Weber 2005; Blakely 1995; Ravat et al. 2007). According to Odegard & Weber (2005), a window of 45 – 55 km is suggested to be optimum for basement depth estimate when working on sedimentary basins, and it should be at least 6times the expected basement depth in the survey area (Salem et al. (2014)).

In the present study, the power spectrum method was applied to the TMI data using Oasis montaj in which the TMI data were transformed from space domain to wavenumber domain using FFT, the radially averaged power spectrum (RAPS) was generated, then marked by three straight lines with slopes that indicate the deeper sources (regional component), shallow sources (residual component) and the noise portion Figure 14.

In order to compute the depth to basement (sediment thickness) in this work, the TMI grid was subdivided into nineteen (19) windows of different size in the suggested window range depending on the observed anomaly contributing to source depth so as to minimize noise and improve basement depth accuracies. The RAPS for each window was calculated from which basement depth was manually computed across the study area by first determining the slope of each RAPS and then plugging its slope into equation (4) to obtain the average depths for the regional and residual components ***Figure 15*** for window one (W1) and other grid windows labelled (W2 - W19) on the study area with their depth populated on the map Figure 16.

3.3.2. Euler Deconvolution Method

The Standard Euler deconvolution method is used to estimate depth and location of magnetic or gravity sources in the Earth`s subsurface. It applies a moving window through the data followed by the least-squares inversion to obtain the depth and horizontal location of magnetic source bodies with different structural indices Barbosa et al. 1999; Thompson 1982); Harris et al. 1996; Hood 1965). The theory of this method has been applied by many scholars including Reid et al. (1990); Reid & Thurston (2014) who recommended that, the most reliable structural index (SI) should indicate the tightest cluster of solutions with linear trends for contact or fault locations and circular cluster solutions for a pipe /cylinder shaped object.

In the present study, the 3D Euler Deconvolution method was applied to the gravity anomaly data using SI of 0 and 1 as supported by Reid et al. 1990 for the aim of delineating and mapping depth to gravity sources. Other parameters used include: survey elevation 120m, maximum depth tolerance 15% and window size 15x15 to map the depth to basement in the study area. The window size was chosen as it lies within the range of 3x3 to 20x20 which can give the best depth estimate to gravity or magnetic sources (Reid et al. 1990; Geosft Inc. 2010; Geosft Inc. 2007). Hence the gravity Euler solution maps were created Figure 17 and Figure 18 then overlaid with the 1VDR and TDR for each SI value chosen. The tightest cluster solutions with linear trends on the maps indicates fault edge boundaries.

4. Results

4.1. Geological Interpretation of Magnetic Data

Geological interpretation of magnetic data can be done by making observations direct from the variations of magnetic intensities and relating them to their possible sources in the survey area. This can be achieved by identifying and demarcating anomaly patterns on the magnetic map as suggested by Telford et al. (1998); Reeves. (2005).

In the present study the RTP-TMI anomaly, RTP-TMI derivatives (1VDRT-RTP-TMI; THD-RTP-TMI and TDR-RTP-TMI) were used to identify and delineate magnetic anomaly zones for geological interpretation of the study area. Two main magnetic anomaly zones were marked on the RTP-TMI map Figure 19, where high magnetic anomalies (zone-A0) ranging between (37.85 - 501.77nT) and lower anomaly (zone-B0) from (-86.47 to 37.00nT). Zone-A0 was subdivided into six sub-zones (A, A1, A2, A3, A4 and A5) while zone-B0 was subdivided into two sub-zones (B1 and B2) Figure 20, Figure 21 and Figure 22.

From (Figure 20, Figure 21 and Figure 22), Zone-A indicates relatively low positive anomaly (38 – 62nT) caused by the kaolinitic rocks (clayey-silt kaolinitic sandstones) of the Mid-Miocene age in the Pugu Hill (Schwaighofer & Muller 1987), close to the shoreline zone-A is overlain by limestone formed in the Mio-Pliocene (Prasad et al. 1982).

Zone-A1 shows high magnetic anomaly (126.86 – 501.77nT) with a linear anticlinal structure, this conspicuous anomaly is probably due to thermally doming salt of the Early-Jurassic age known from seismic evidence and borehole information in the Mandawa Salt Basin (Kent et al.1971; Hudson & Nicholas 2014; Said et al. 2015). Zone-A2 shows high magnetic anomaly (80 – 501.77nT) south of the Wingayongo Hill, this is probably due to the existing local intrusive from hot spring found in the Rufiji valley while towards the Matumbi Hill in this zone, high anomalies may suggest the presence of dykes, sills of phonolites and dolerites of the Eocene age formed during the EARS (Kreuser et al. 1990) as well as the effects of metamorphic and igneous rocks extended from the Massasi Spur Basement (Kent et al. 1971; Hudson & Nicholas 2014; Said et al. 2015). Zone-A3 indicates high anomaly west of the Mandawa Salt Basin, part of the Selous Basin and northwest of the Rufiji Depression, these anomalies may suggest the effect of metamorphic and igneous rocks of the Massasi Spur Basement known from the geology of the study area Figure 1. Zone-A4 shows high anomalies in the offshore to the east border of the Rufiji Depression due to the Davie ridge fracture zone of the intrusive igneous rocks formed during the Karoo II rift system (Causebrook and Archer 1979; Watson & et al. 2012). Zone-A5 indicates high magnetic anomaly to the north of the Rufiji Depression probably due to the presence of volcanic intrusion found in the area (Kent et al. 1971; Spence 1957).

Zone-B1 and B2 shows negative magnetic anomaly associated with a thick crust in the range of (2.3 - 10.5 km) thickness overlying the basement Figure 16. This crust thickness is attributed to the fluvial deltaic sediments deposited from the Rufiji River in the central part of the study area westwards and clastic marine sands from the Mafia Channel (Kent et al. 1973)

towards the WSSB. These sediments are predominantly Neogene in the Rufiji Depression northwards resting on top of the Karoo shale sediments of the Jurassic age.

4.1. Geological Interpretation of Gravity Anomaly Data

Gravity anomaly maps are used to illustrate density contrast variations related to deeper seated geological bodies within the subsurface. In this study, gravity anomaly maps were created and marked with zones according to their distinctive anomalies Figure 9 and (Figure 11, Figure 12 and Figure 13). Zone-D1 indicates high gravity anomaly probably due to deeper seated Jurassic rocks overlying the basement, toward the Matumbi Hill the highs gravity anomalies are probably caused by the presence of dykes of the Eocene age (Kreuser et al. 1990) and the effect of basement rocks that extends from the Massasi Spur (Kent et al. 1971).

The high gravity anomaly on Zone-D2 may suggest the existence of volcanic intrusive rocks available in the region (Kent et al. 1971, Spence 1957). Zone-D3 high gravity anomaly may indicate the exposed edge of the basement that coincide with the edge of the Rufiji Trough parallel to the fault trending W – E from the Ngerengere graben while the low anomaly in Zone-E1 to the south are probably due to the presence of thermally doming salt which has low density contrast as compared to Jurassic rocks in the Mandawa Salt Basin (Hudson & Nicholas 2014). Zone-E1 indicates a low gravity anomaly trending E-W, this may suggest the presence of hot spring and new deposited sediments along the Rufiji Valley, while low gravity anomaly zone-E1 to the north-east is caused by the presence of low density contrast of limestone sediments available in the region (Kent et al. 1971).

Generally, the observed features from gravity results in the present study have indicated a good correlation with geological bodies available on both topographic Figure 3 and geological maps of the study area Figure 1.

4.2. Revealed Geological Structures from Magnetic and Gravity Data Results

The RTP-TMI derivatives (Figure 20, Figure 21 and Figure 22) and gravity Euler solutions Figure 17 and Figure 18 were combined and utilized to delineate geological structures in the study area. Results has indicated the major linear geological structures in the area which were interpreted as regional faults. These structures were delineated and mapped with trends: NNW-SSE, NNE-SSW, N-S and some relatively W-E direction Figure 23.

Deduced results from this study are reliable as they are consistent to the geology of the study area and have indicated good correlation with previous results from other geological studies (e.g Kapilima 2002; Kent et al. 1971; Said et al. 2015).

Additionally, this study has also identified some new linear geological features (orange colour) in the Massasi Spur basement from magnetic data and other curved solid blue lines in the Dar es Salaam Platform, Rufiji Depression and Mandawa Salt Basin all delineated from gravity Euler solutions Figure 17 and Figure 18.

4.3. Estimated Basement Depth Results

The power spectrum and Standard Euler deconvolution methods were applied to compute depth to magnetic and gravity causatives respectively. The power spectrum results indicate estimated regional basement depths of the study area ***Figure 16***. Results are likely reliable since they have indicated good correlation with sediment distributions across the study area as described in section 4.1 and 4.2.

Also, the gravity Euler solutions depth were computed for basement depth comparison with the power spectrum results. However, the gravity Euler solutions depth results Figure 17 and Figure 18 observed to be consistent with the power spectrum ones across the study area since results from both methods have indicated relatively similar depth ranges.

5. Discussion, Conclusion and Recommendations

5.1. Discussion

From magnetic and gravity data results, the study has successfully delineated, mapped and revealed the W- E buried Neogene faults running from the Ngerengere basement through the edge of Rufiji River, the Early-Jurassic faults trending NNW-SSE from the Mandawa Salt Basin, NEE-SWW running parallel to the north of the Massasi Spur Basement, and the Karoo faults trending NNW-SSE, and NNE-SSW Figure 23 which are relatively similar to those identified from previous studies using gravimetric and isopachs data around the Coast Basin of Tanzania (Kapillima 2002). Kent et al. (1971). Gravity results revealed some new regional structural trends (Neogene faults) in the Dar es Salaam Platform and Rufiji Depression with major trends: W-E, N-S, and NNE – SSW which were attributed to the EARS.

This work has also detected and mapped the most prominent features such as; hot spring in the Rufiji Valley south of the Wingayongo Hill, anticlinal features of the Early-Jurassic Mandawa salt dome, metamorphic and igneous rocks associated with the Massasi Spur Basement and dykes of the Eocene age in the Rufiji Depression, Kaolinitic rocks formation of Pugu Hills and volcanic rocks intrusion north of the Rufiji Depression, which were all indicated by high magnetic anomaly and tremendous sediment thickness varying from (2.3 ± 0.8 – 10.5 ± 0.8)km depth with mainly low magnetic anomaly across the study area Figure 16, Figure 20, -Figure 22.

Results from the revealed features are in good agreement with the geology of the study area as well as those from previous geological studies by Hudson & Nicholas. (2014), Kent et al. (1971), Hudson et al. (2011) in the Coast Basins of Tanzania. Also, magnetic results revealed some structural trends (orange colour) Figure 23, in the Massasi Spur Basement.

5.2. Conclusion

Two datasets (gravity and magnetic data were utilized in this study to delineate regional geological structures, map basement depth of the Rufiji Depression area. The geological structures like faults, salt dome, dykes, hot spring intrusion and sedimentary basin boundaries were identified, delineated and mapped using the RTP-TMI derivatives (1VDR, THD, TDR), BA, BA-residual, and both TDR and 1VDR of residual-gravity data. Basement depth to magnetic sources was mapped using the Power Spectrum while due to gravity causatives by Standard Euler Deconvolution method. The regional depth to basement was estimated in the range of (2.3 ± 0.8 – 10.5 ± 0.8) km from the power spectrum results while those from Standard Euler Deconvolution method were found in the range of 2km– to more than 8.0km depth across the study area. Depth to basement results are considered reliable as they are relatively consistent from both methods and are in good agreement with the geology and topography of the study area.

5.3. Recommendations

Regional geological structural trends were successfully delineated and mapped using potential field data regardless its relatively poor resolution, but some known geological features were not revealed in the study area. However, in order to efficiently constrain the geological features of the Rufiji Depression and its vicinity, high resolution potential field data should be utilized. The study has revealed thick to thinner sediment distributions under the application of potential field data. In order to correlate the depth to basement results of the present study, further studies should be conducted by probably integrating both high resolution potential field and seismic data across the study area.

6. Acknowledgement

I thank God for his power, passion, care and blessings for taking me safely during this course. My special recognition goes to my supervisor Prof. Stephenson Randell. A, for his guidance and tireless advice during my project may the almighty God bless him for his zeal and constructive comments to make this project possible. My sincere acknowledgement goes to my employer the TPDC Managing Director Dr. James Mataragio for his funding support and permission to allow me carry out this course. I also thank the Geophysics Department of the University of Aberdeen for providing me with the Software Oasis montaj, ArcGIS and Petrel packages as this project could be intractable without these facilities. My final gratitude goes to my wife ***Abia Selemani***, my kids ***Evance*** and ***Evelyn*** for their prayers and advice during this course, may God bless them all.

7. References

i. Atawa, M., Zouaghi, T & Souei, A. (2016). Gravity constraints on the underground structural framework and associated volcanism of the Maghrebian allochthonous domain: The Sejnene Numidian flysch, Tunisian Tell. 116, 248 - 263.
ii. Barbosa, V., Sliva, J & Medeiros, W. (1999). Stability analysis and improvement of structural index in Euler deconvolution. Geophysics, 64, 1999, 48-60.
iii. Blakely, R. (1995). Potential theory in gravity and magnetic applications, Cambridge University Press, 441p.
iv. Blakely, R.J. (1996). Potential Theory in Gravity and Magnetic Applications. Cambridge University Press, UK (445 p.).
v. Briggs, I.C., (1974). Machine contouring using minimum curvature. Geophysics 39, 39-48.
vi. Causebrook, R. M & Archer, D. W. (1979). The Geology and Hydrocarbon Prospects of the Songo songo Field. Tanzania.
vii. Cooper, G.R.J., Cowan, D.R., (2004). Filtering using variable order vertical derivatives. Comput. Geosci. 30, 455–459.
viii. Connard, G., Couch, R & Gempert, M. (1983). Analysis of aeromagnetic measurements from the cascade-range in central Oregon. Geophysics, 48: 376 – 390
ix. Fairhead, J. D., C. M. Green, B., Verduzco, & MacKenzie, C. (2004). A new set of magnetic field derivatives for mapping mineral prospects: 17th Geophysical Conference, ASEG, Extended Abstracts.
x. Geosoft Inc (2015). Applying Fast Fourier Transform MAGMAP. www.geosoft.com/resources/goto/applying-fast-fourier-transform-magmap
xi. Harris, E., Jessell, W., & Barr, T. (1996). Analysis of the Euler deconvolution techniques for calculating regional depth to basement in area of complex structures. SEG Ann. Intern. Meeting.
xii. Hood, P., 1965, Gradient measurements in aeromagnetic surveying: Geophysics, 30, 891–902.
xiii. Hudson, W.E & Nicholas, C.J. (2014). The Pindiro Group (Triassic to Early Jurassic Mandawa Basin, southern coastal Tanzania): Definition, palaeoenvironment, and stratigraphy. Journal of African Science. 92, 55 – 67.
xiv. Kapilima, S. (2002). Tectonic and Sedimentary Evolution of the Coastal Basin of Tanzania during the Mesozoic times.
xv. Jacoby, W., Smilde, P.L. (2009). Gravity Interpretation: Fundamentals and Application of Gravity Inversion and Geological Interpretation. Springer-Verlag, Berlin Heidelberg (387 p).
xvi. Kent, P.E., F.R.S., Hunt, M.A & Johnstone, M.A. (1971). The geology and geophysics of coastal Tanzania. London.

xvii. Kreuser, T., Wopfner, H., Kaaya, C.Z., Markwort, S., Sekiwa, P.M and, Aslanidis, P (1990). Depositional evolution of Permo-Triassic Karoo basins in Tanzania with reference to their economic potential. J. African Earth Sciences. 10, 151 – 167.

xviii. Lamotte, D. F, Leleu, S, Francois, L & Clarens, P. (2015). Style of Rifting and Stages of Pangea Break-up. Tectonics, 34, doi: 10.1002/2014TC003760.

xix. Miller, H.G., Singh, V. (1994). Potential field tilt — a new concept for location of potential field sources. J. Appl. Geophys. 32, 213–217.

xx. Nayak, G.K & Petkovic, P. (2011). Depth to Magnetic Basement of the Capel and Faust Basins, Lord Howe Rise.

xxi. Odegard, M.E & Weber, W.R. (2005). Depth to basement using spectral inversion of magnetic and gravity data: application to Northwest Africa and Brazil. University of Houston and Dickson International Geosciences. Internal report.

xxii. Phillips, J.D. (2000). Locating magnetic contacts: a comparison of the horizontal gradient, analytic signal, and local wavenumber methods. SEG 2000, Expanded Abstracts.

xxiii. Phillips, J.D. (1998). Processing and interpretation of aeromagnetic data from Santa Cruz Basin-Patahonia mountains area, south-central Arizona. US Geological Survey Open-File Report, pp. 02–98.

xxiv. Prasad, G.I., Dixit, P.C & Nanyaro, J.T. (1982). Preliminary study of the Wazo Hill limestone. Dar es Salaam. Sci, J. 7, 177-131.

xxv. Reeves, C. (2005). Aeromagnetic Survey; Principles, Practice and Interpretation. Geosoft.

xxvi. Reid, B., Allsop, J.M., Granser, H. Millet, A.J & Somerton, I. W. (1990). Magnetic interpretation in three dimensions using Euler deconvolution. Geophysics. Vol. 55, No. I; P. 80-91.

xxvii. Said, A., Moder, C., Clark, S & Abdelmalak, M. M. (2015). Sedimentary budgets of the Tanzania coastal basin and implications for uplift history of the East African rift system. Journal of Africa Earth Science 111, 288 - 295.

xxviii. Salem, A., Green, C., Ravat, D., Singh, K.H., East, P., Fairhead, J.D., Mogren, S., & Biegert, E. (2014). Depth to Curie temperature across the central Red Sea from magnetic data using the de-fractal method. Tectonophysics, 75 – 86.

xxix. Schwaighofer, B & Muller, H.W. (1987). Mineralogy and genesis of the Pugu Hill Kaolin Deposit Tanzania. Clay Mineral, 22, 401-409.

xxx. Sheriff, R.E. (2002). Encyclopedic dictionary of applied Geophysics. 13 Geophysical Reference Series, 4th edition Society of Exploration Geophysicists, Tulsa USA (429 p).

xxxi. Spector, A., & Grant F. S. (1970). Statistical models for interpreting aeromagnetic data. Geophysics, 35: 293-302.

xxxii. Stephenson, R.A., Ricketts, B.D. (1990). Bouguer gravity anomalies and speculations on the regional structure of the Eurekan Orogen, Arctic Canada.

xxxiii. Telford, W.M., Geldart, L.P., Sheriff, L.E. (1990). Applied Geophysics, second ed. Cambridge University Press, pp. 62e135 (Chapter 2): Gravity methods, 6e61. (Chapter 3): Magnetic methods.

xxxiv. Thompson, D. T. (1982). EULDPH: A new technique for making computer-assisted depth estimates from magnetic data, Geophysics, 47, 31-37.

xxxv. Watson, J. G., Glover, C. T., Munoz, A. A., Harris, J. P., Goodrich, M & Fugro Robertson Limited. (2012).

xxxvi. The Evolution of the Offshore East African Margins and Intracontinental East African Rift: A Combined Rigid/Deformable Tectonic Reconstruction. Llandudno, North Wales, LL30 1SA, UK.

xxxvii. Verduzco, B., Fairhead, J.D., Green, C.M., Mackenzie, C. (2004). New insights into magnetic derivatives for structural mapping. Lead. Edge 23, 116–119.

Appendix

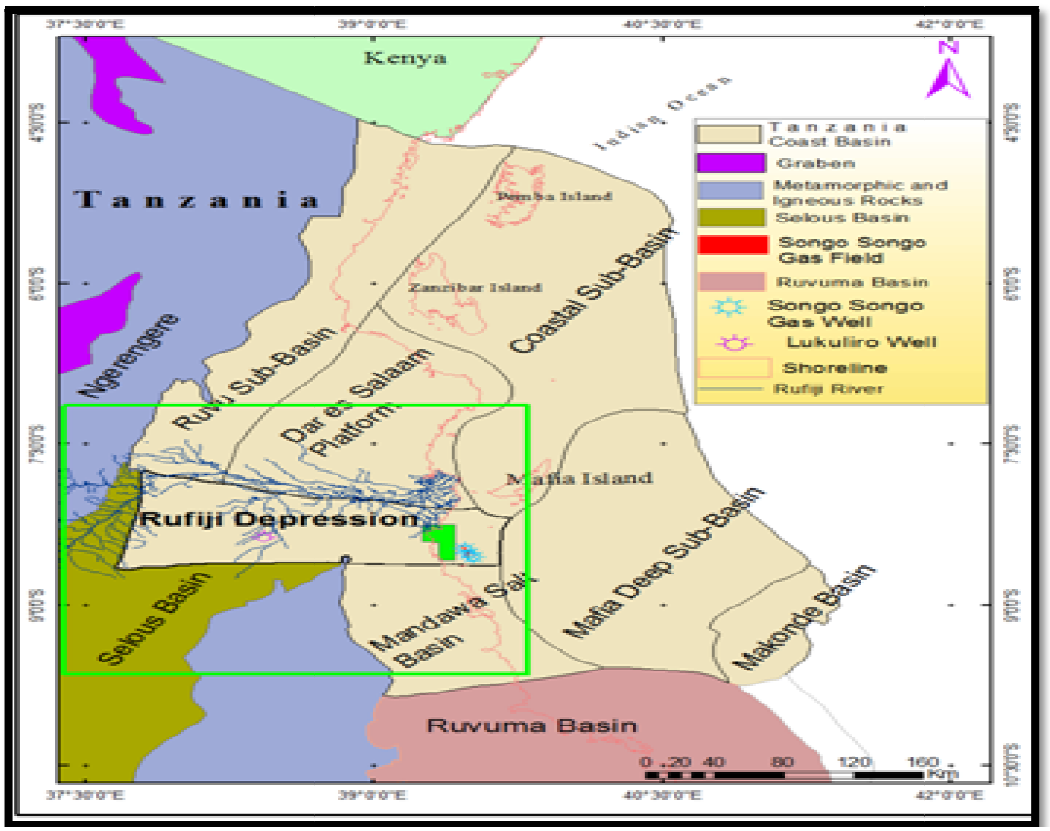

Figure 1: Location map of the coast basins of Tanzania created using ArcGIS Software, the green box on the map represent the study area while the solid green area is the WSSB

Figure 2: East Africa Tectonic Setting (After Lamotte Et Al. 2015)

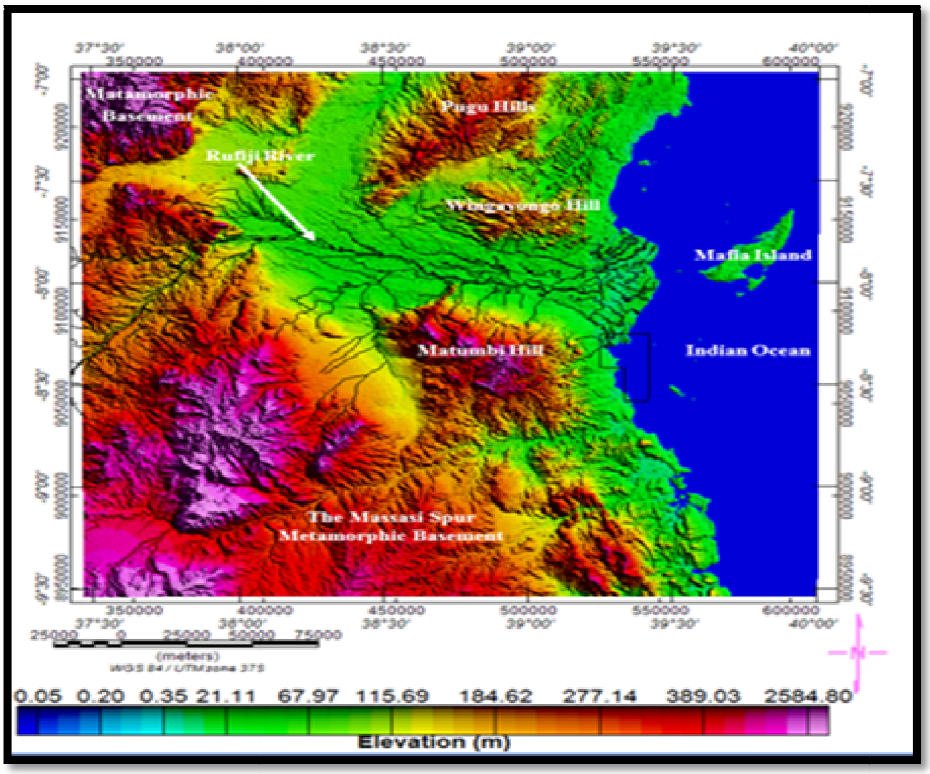

Figure 3: Topographic Map of the Study Area Created Using Oasis Montaj, Dataset Used Were Extracted from SRTM Link of the Geosoft Public Server

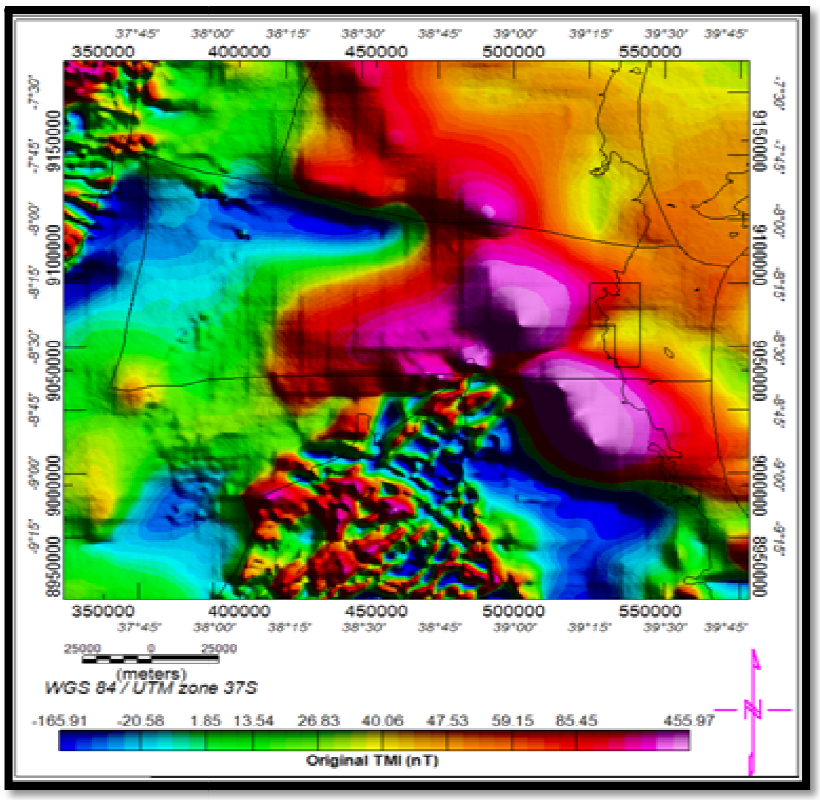

Figure 4: The Map of the Original TMI Anomaly Data before Application of Filters and Enhancement Strategies on It, the Black Line on All Magnetic and Gravity Maps Signifies The Sedimentary Basin Boundaries of the Study Area (Not Geological Structures)

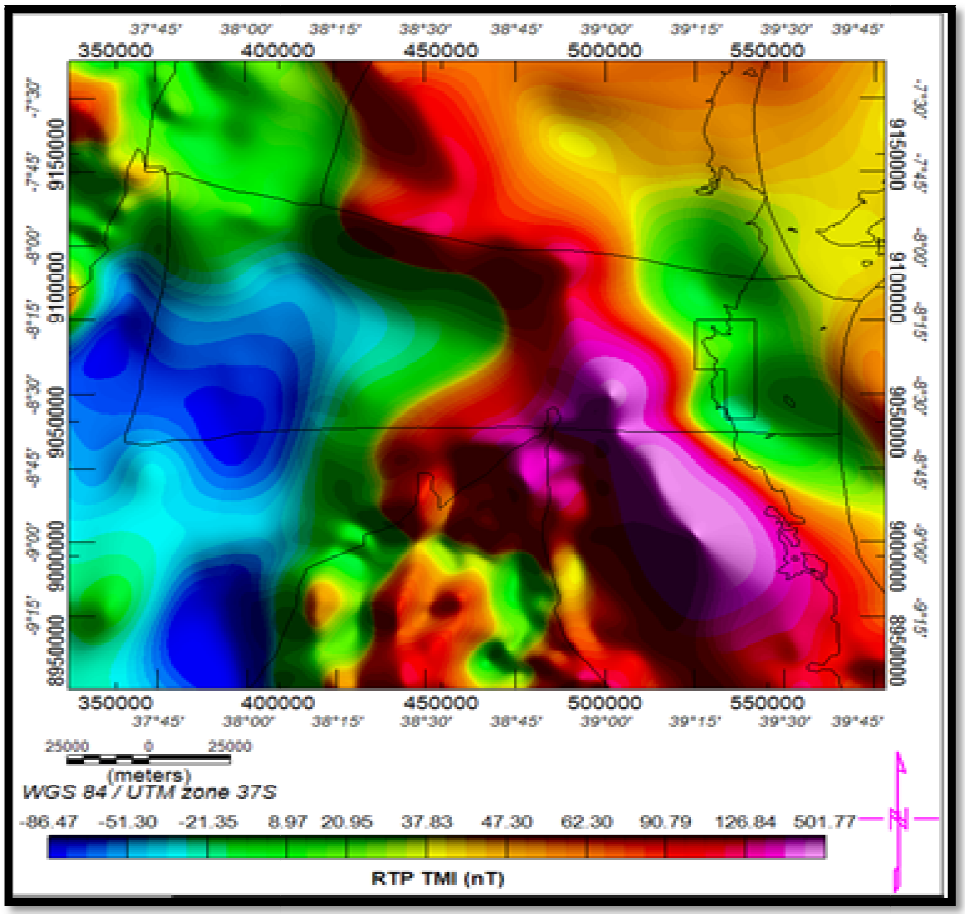

Figure 5: The Map of the RTP-TMI Anomaly, the Centres of Magnetic Anomaly is Enhanced and Directly Oriented above the Magnetic Sources with Respect to the Direction of the Geomagnetic Pole The RTP-TMI Data Indicate a Conspicuous Positive Regional Magnetic Lineament Trending NNW-SSE across the Study Area and Others Trending N-S in the Study Area

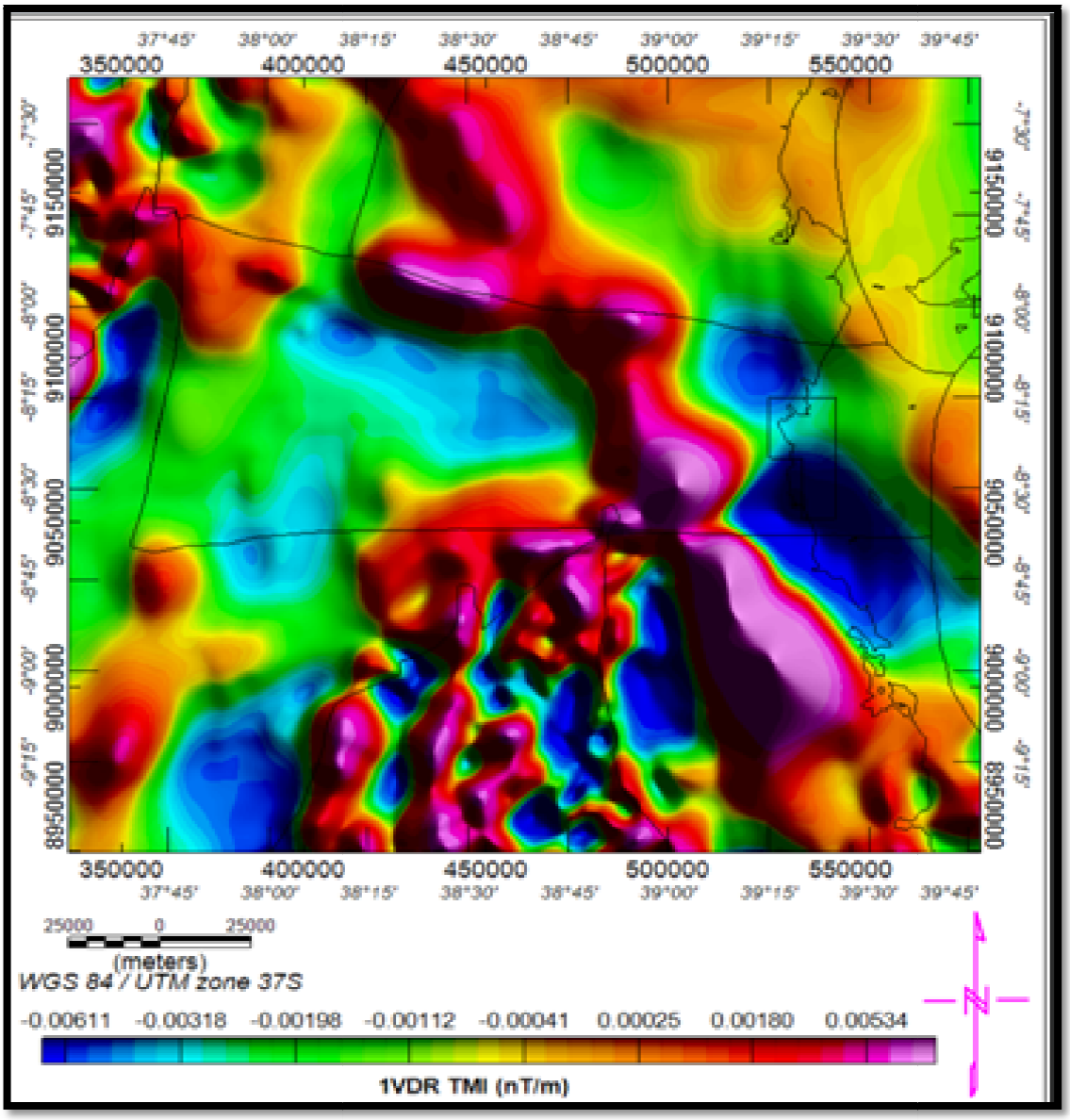

Figure 6: The Map Showing the First Vertical Derivative of the RTP-TMI, Short Wavelength-Anomalies (Shallow Magnetic Causatives) are more accentuated on the Map. Also, the Edges of Maxima High Magnetic Anomalies with Linear Features Related to Geological Body Contacts or Boundaries are More Emphasized on The Map

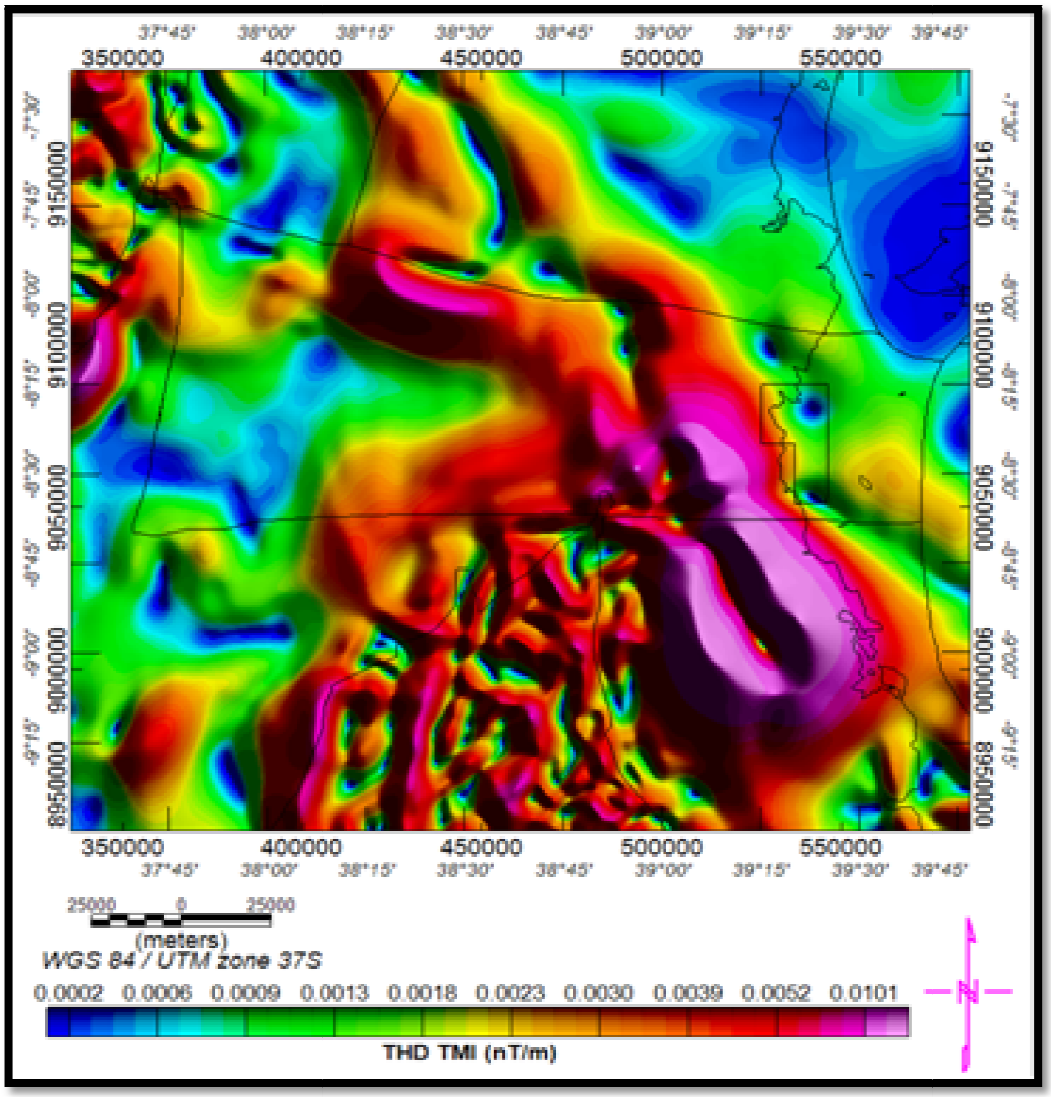

Figure 7: The THD of the RTP-TMI Anomaly Map Showing Clear Edges Contact Locations of Linear Geological Structures with High Magnetic Anomalies in the WSSB, the THD Magnetic Anomaly Map Produced Is Plausible and Enough for the Intended Geological Interpretation

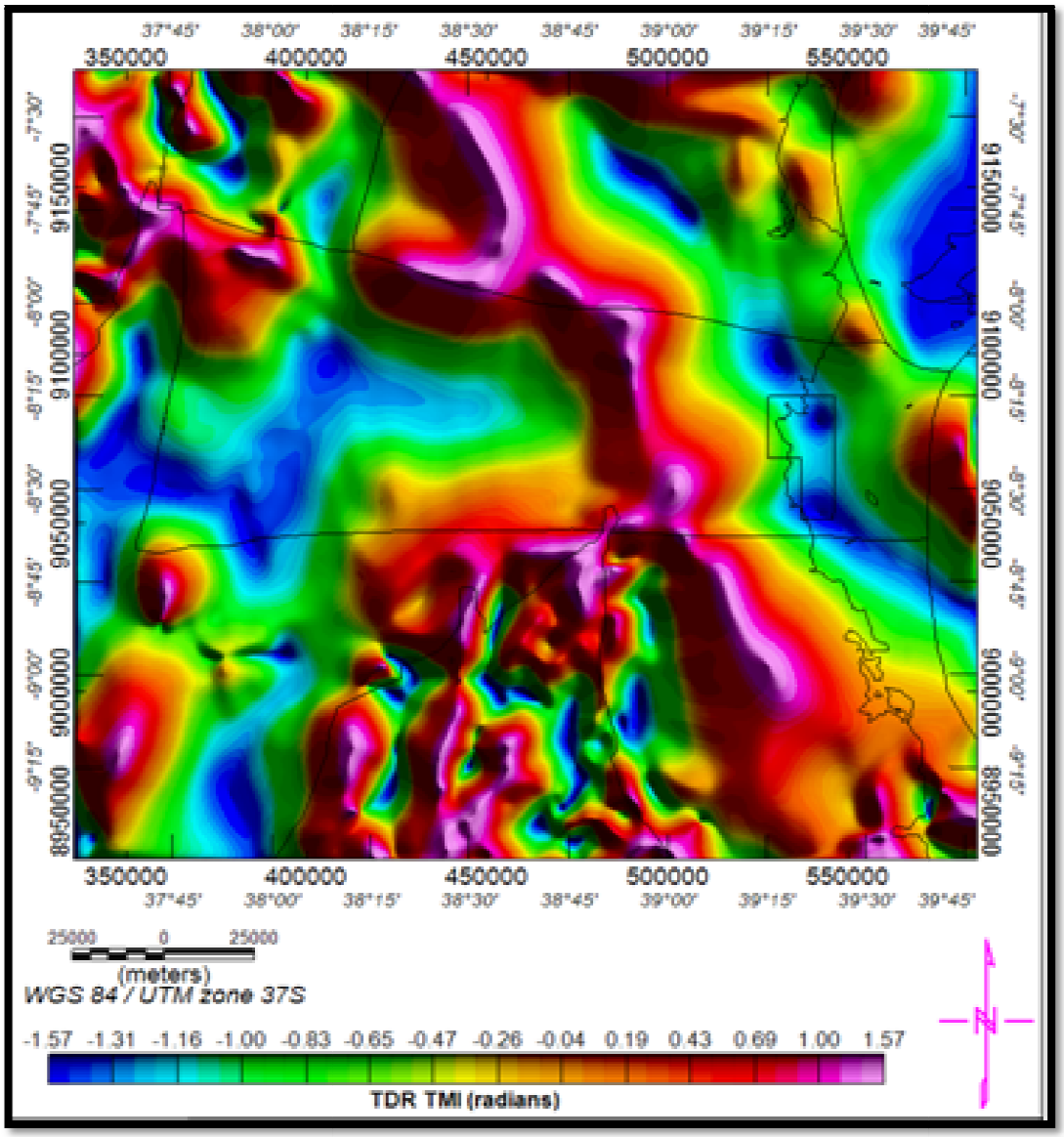

Figure 8: A Map Showing the Tilt Derivative of the RTP-TMI Anomalies. The Continuity of Linear Geological Bodies (High Anomaly) Is Highly Emphasized and Edges of Magnetic Causatives are Accentuated

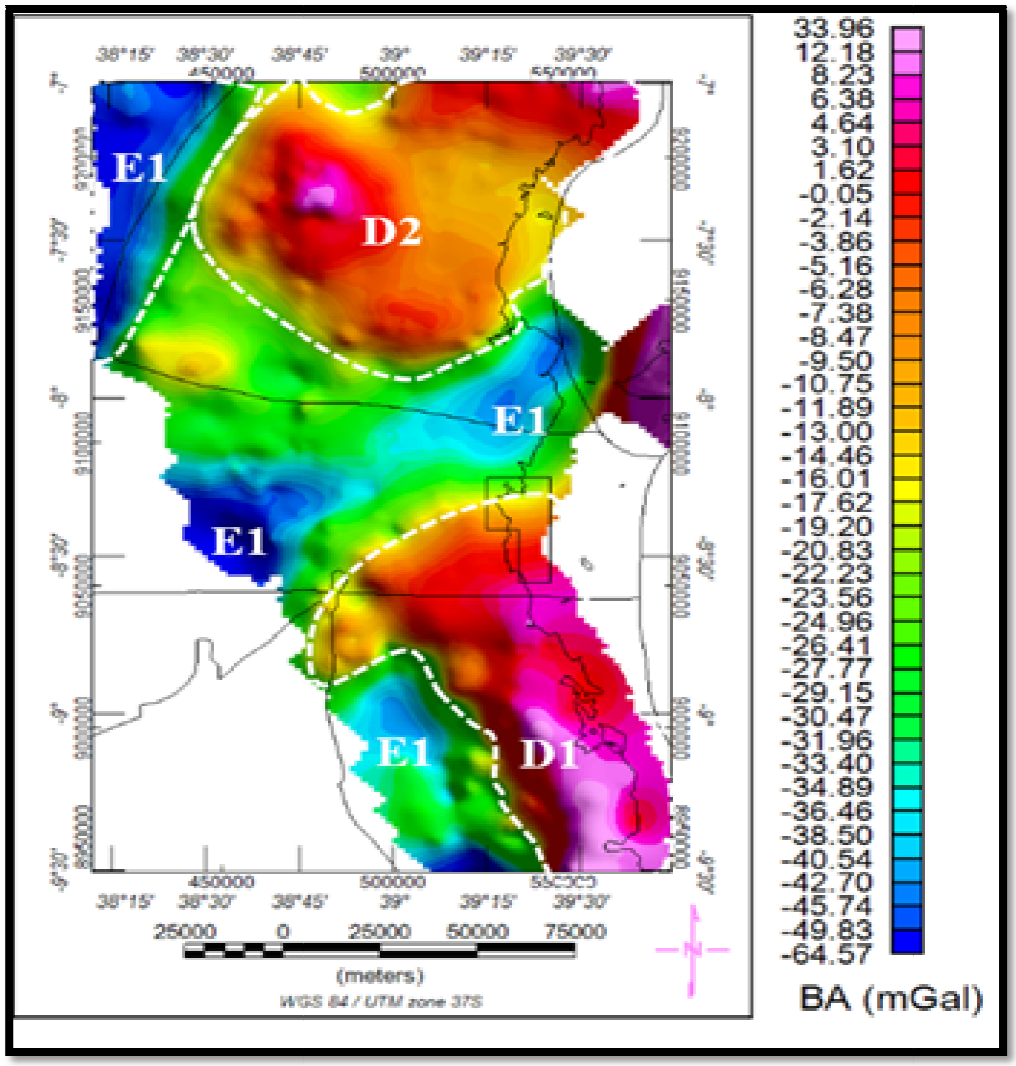

Figure 9: The Gravity Bouguer Anomaly Map of the Study Area, Zones Related to High (D1- D2) and Low (E1) Gravity Anomalies are Marked and Delineated on the Map

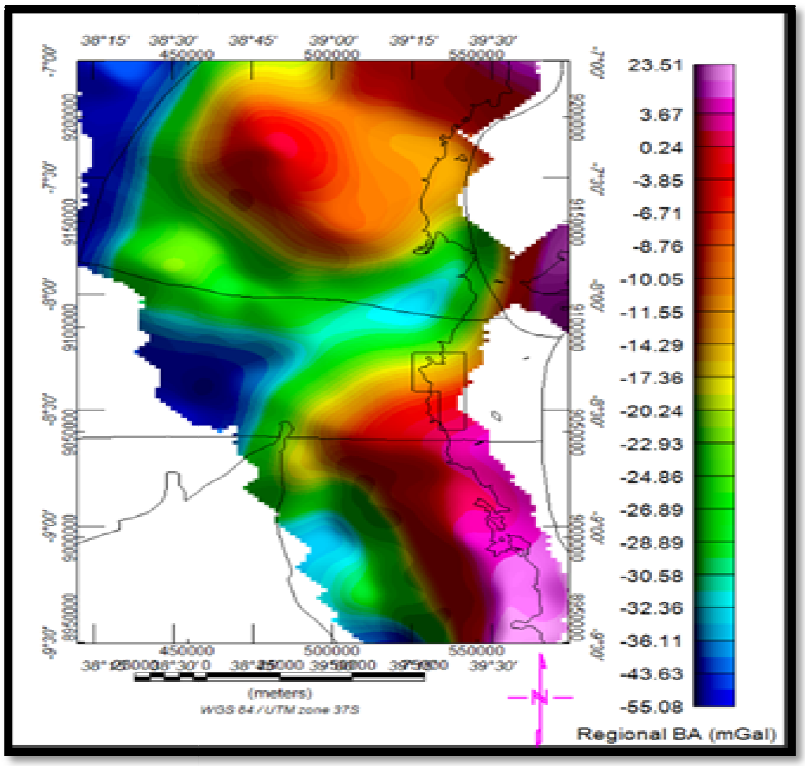

Figure 10: The Regional Gravity Anomaly Map Showing Density Contrast Variations of Geological Features in the Study Area

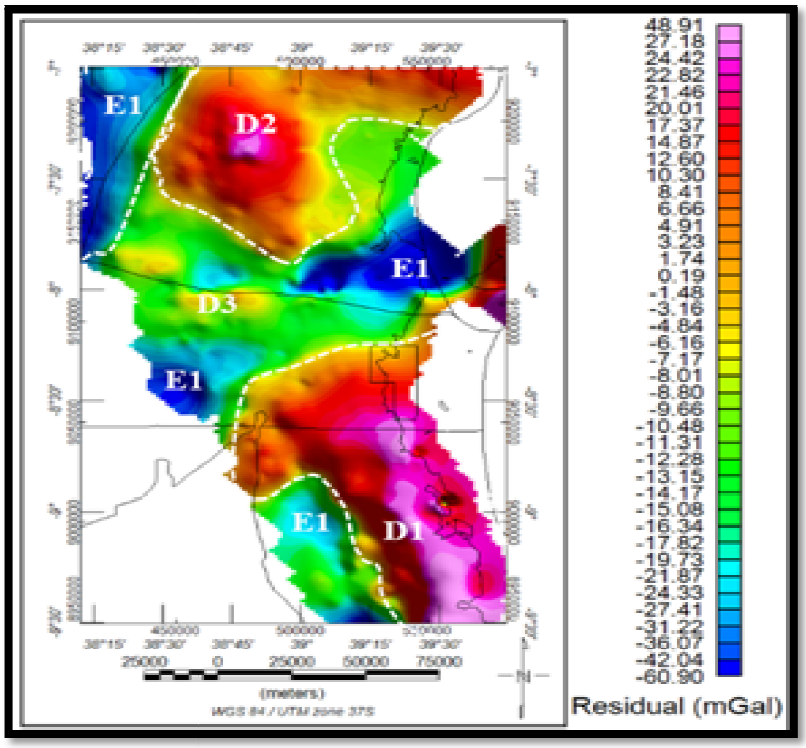

Figure 11: The Residual Anomaly Map of Gravity Data, the High (D1- D3) and Low (E1) Gravity Anomaly Zones are Marked and Delineated on the Map. The Mapped Structures Indicate a Good Correlation to the Geological Features Existing in the Study Area which are Critically Analyzed in Section 4.2

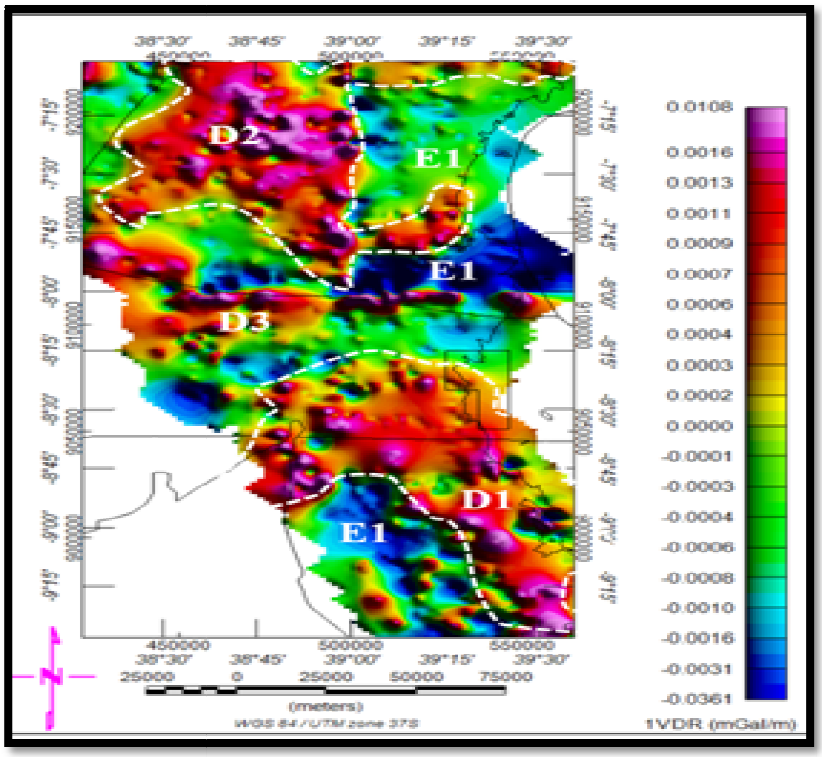

Figure 12: The 1VDR of the Residual Gravity Anomaly Map of the Study Area, The High (D1- D3) and Low (E1) Gravity Anomaly Zones are Marked on the Map from which the Shallow Geological Bodies of the Crust are Greatly Enhanced and Well Delineated

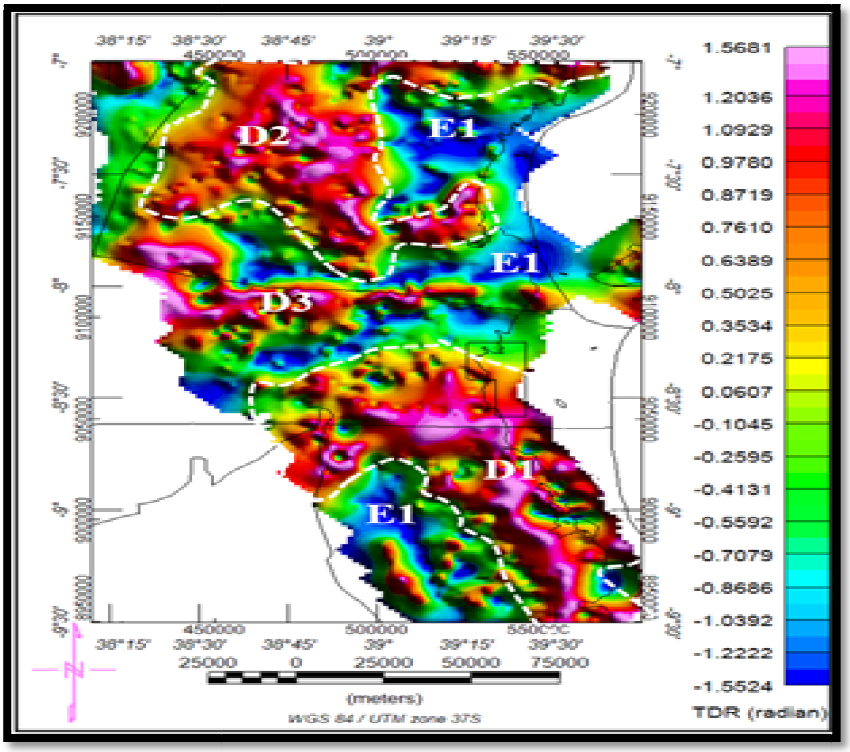

Figure 13: The TDR Derivative of the Residual Gravity Anomaly Map of the Study Area, the High (D1- D3) and Low (E1) Gravity Anomaly Zones Are Marked and Delineate on the Map

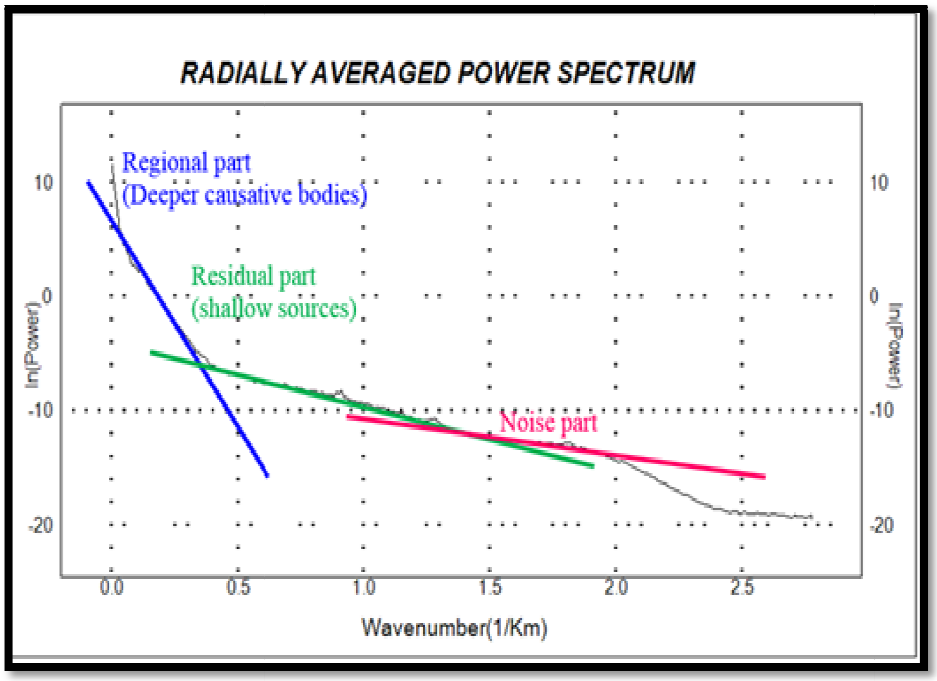

Figure 14: The Radially Averaged Power Spectrum Indicating Three Parts of Magnetic Causative in the Study Area (Regional, Residual and the Noise Portion)

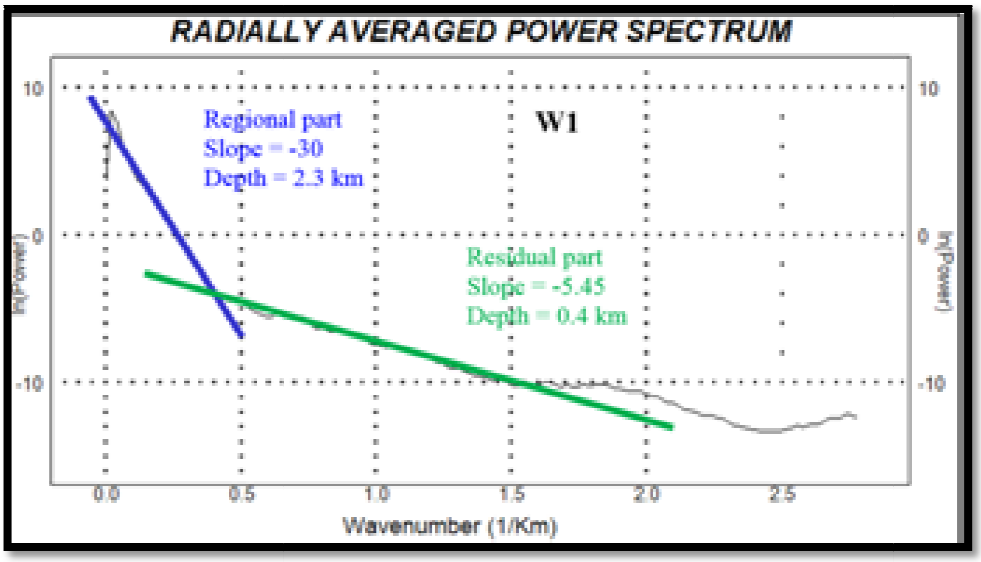

Figure 15: The RAPS Showing Basement Depth Estimate for W1 Whose Location Is Shown in (Figure 16), the Regional Basement Depth after Subtracting Flight Height Effects (120 M) in the Figure above Was Found to Be 2.3km

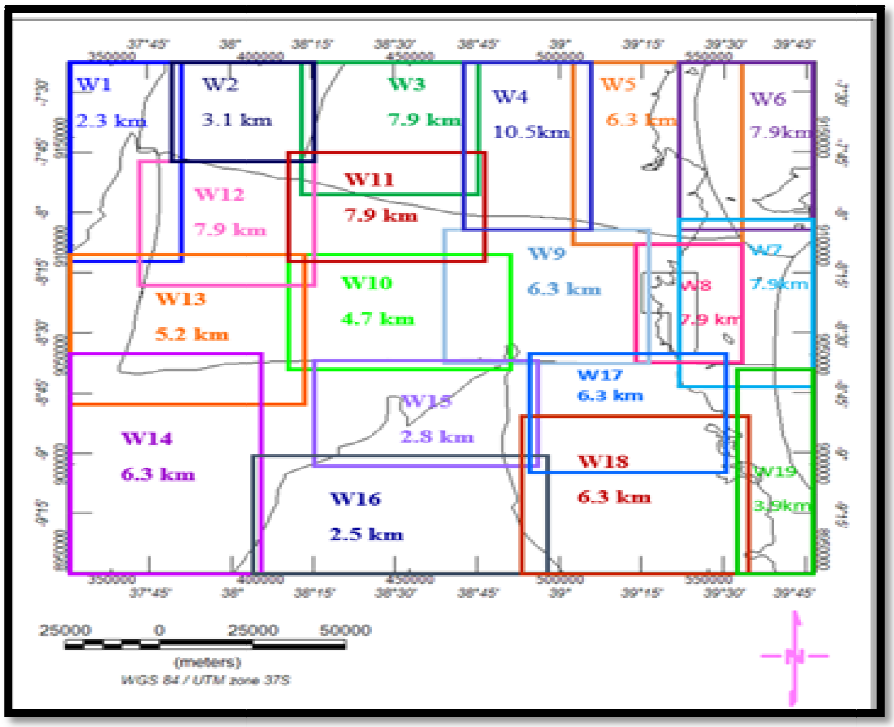

Figure 16: The Map Showing Regional Depth to the Basement of the Study Area, the Depth Values Populated in the Figure Were Compiled from W1 – W19 Using the Same Procedure as Used in (Figure 15)

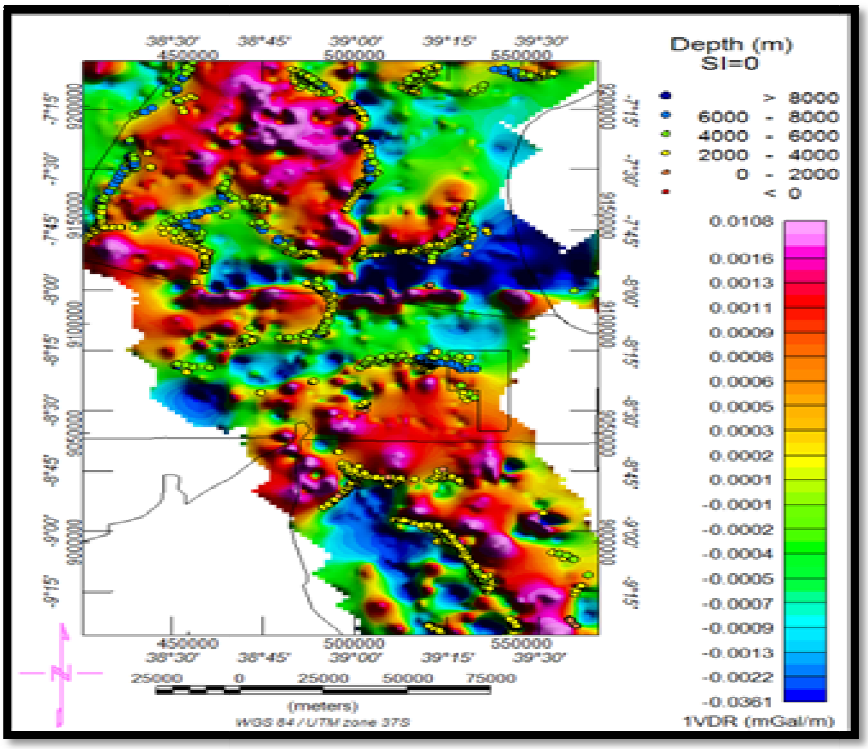

Figure 17: Euler Clustered Solution Map (SI = 0) Overlaid with the 1VDR Gravity Anomaly Data, the Solution Indicates Good Edge Contact with Linear Trends along the Mapped Fault Boundaries from RTP-TMI Derivatives

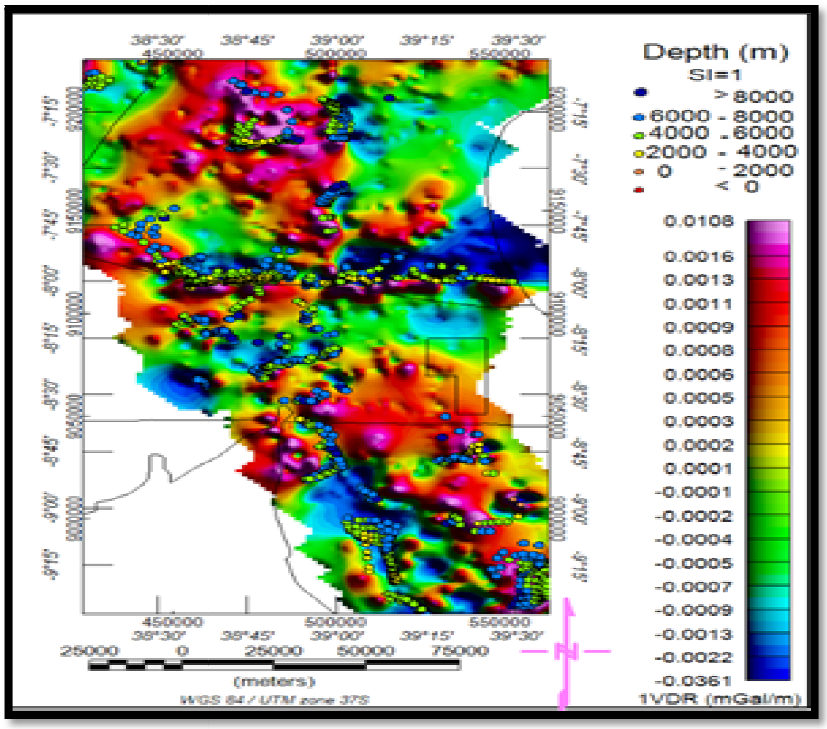

Figure 18: Euler Clustered Solution Map (Si = 1) Overlaid with the 1vdr of the Gravity Anomaly Data, the Tightest Cluster of Solutions on the Map Indicates a Good Edge Contact with the Linear Structural Trends along the Mapped Fault Edges from Magnetic Data

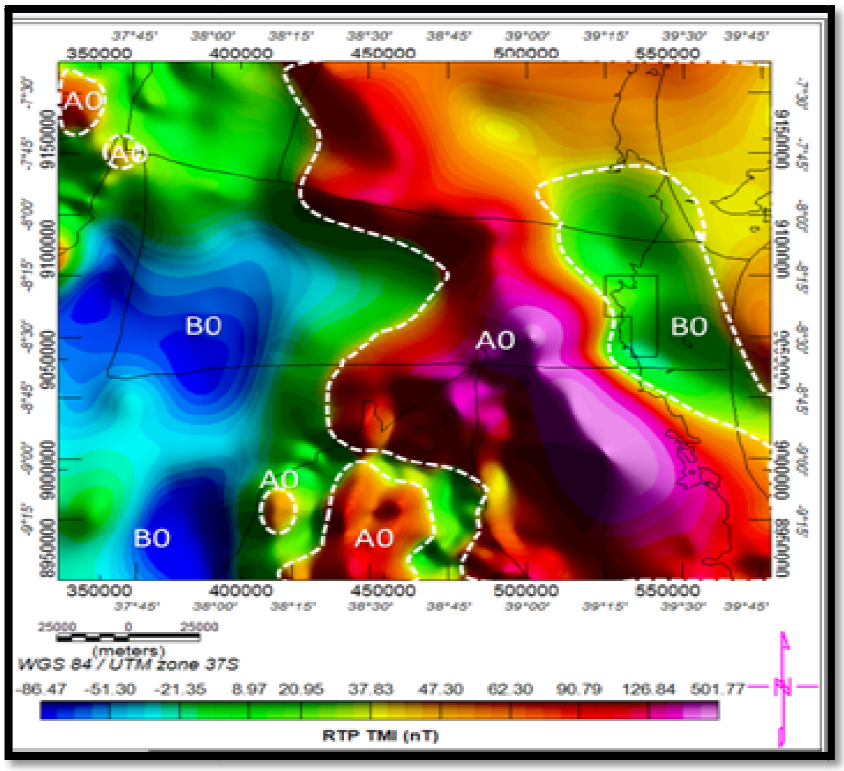

Figure 19: The RTP-TMI Anomaly Map of the Study Area Showing Two Main Magnetic Anomaly Zones (A0-Highs) and (B0-Low), It Was Later Enhanced to Delineate Geological Structures of the Study Area (Figure 20-22)

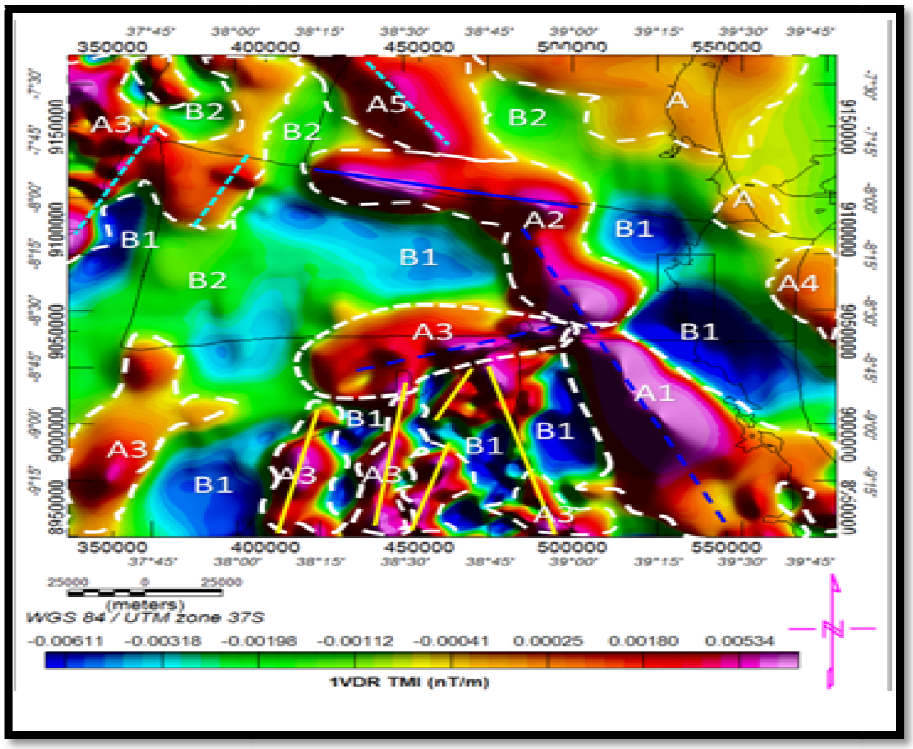

Figure 20: The Map Showing the 1VDR of the RTP-TMI, Short Wavelength-Anomalies (Shallow Magnetic Causatives) are more accentuated in the Figure, Geological Body Contacts Related to Faults are also well delineated and marked by (Dashed Blue, Solid-Blue, Dashed-Cyan) Lines (Figure 20-22)

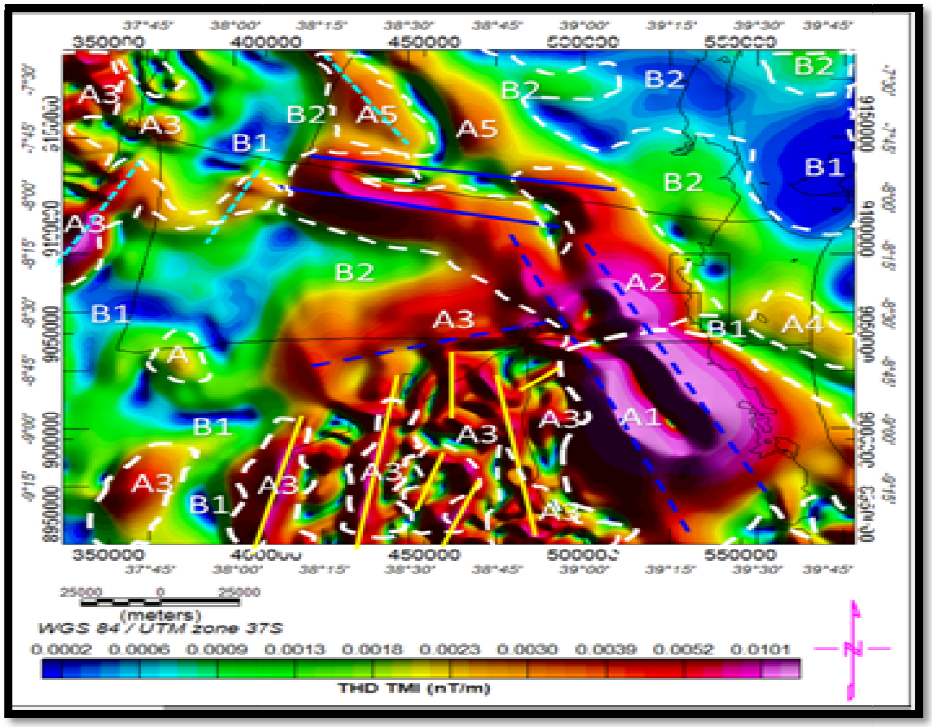

Figure 21: The THD of the RTP-TMI Anomaly Map Showing Conspicuous Edge Contact Locations of Fault Structures in (Dashed Blue, Solid-Blue, and Dashed- Cyan) Lines, Sedimentary Basins (Low) and High Magnetic Anomaly Features of the Study Area

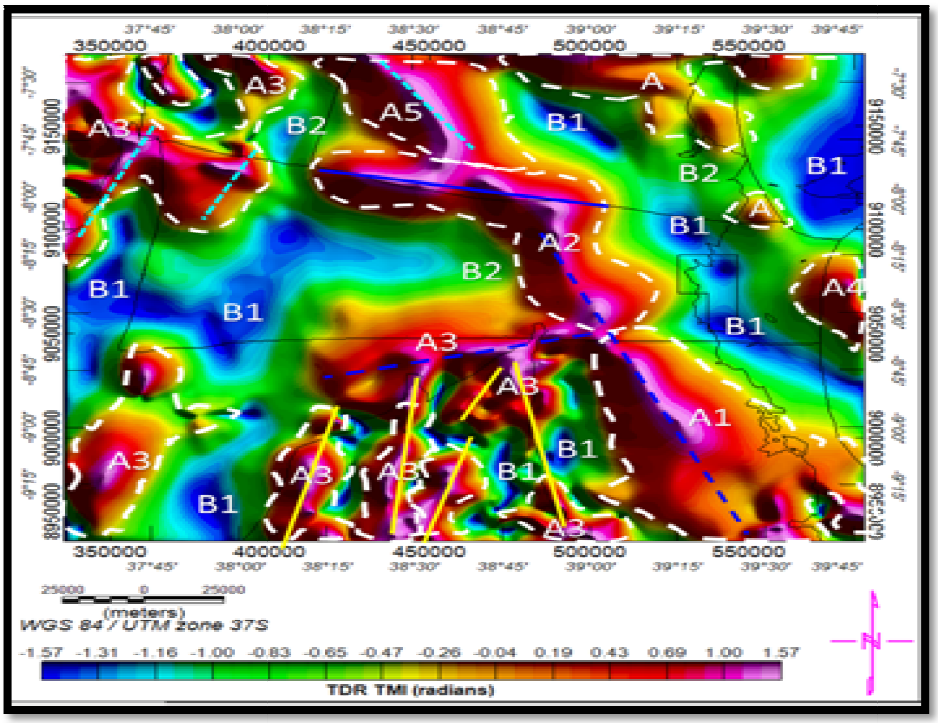

Figure 22: The Map of the TDR of the RTP-TMI Showing Fault Edge Boundaries (Dashed Blue, Solid-Blue and Dashed-Cyan) Lines as Well as the Enhanced Continuity of Geological Structures While Noise Related to Magnetic Anomalies are Highly Attenuated

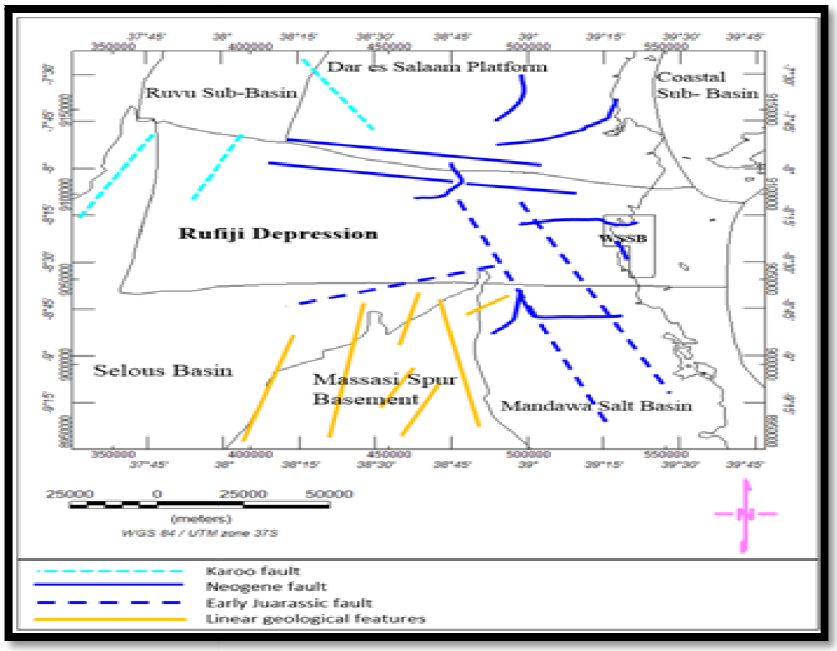

Figure 23: The Map of the Study Area Showing Regional Structural Trends Mapped and Delineated from both Gravity (Figure 17, Figure 18) and Magnetic Data (Figure 20- 22), The NNW-SSE Trends are Attributed to the Early-Jurassic Rifting (Lindi Faults) and NNE-SSW by the Karoo Rifting (Tanga Faults) (Figure 2), While the Feature Trends in Solid Blue Line (Relatively Oriented: W-E, N-S, and NNE – SSW) are Associated with The Youngest Ears (Neogene Faults), the Orange Colour Features Are the New Revealed Structures in the Study Area